International Journal of Heat and Mass Transfer 52 (2009) 6000–6011

Contents lists available at ScienceDirect

International Journal of Heat and Mass Transfer

journal homepage: www.elsevier.com/locate/ijhmt

Transient behavior of run-around heat and moisture exchanger system. Part I: Model formulation and verification

Mehran Seyed-Ahmadi [1], Blake Erb [2], Carey J. Simonson [*,3], Robert W. Besant [4]

Department of Mechanical Engineering, University of Saskatchewan, 57 Campus Drive, Saskatoon, SK, Canada S7N 5A9

ARTICLE INFO

Article history:
Available online 8 September 2009

Keywords:
Transient
Run-around exchanger
Heat and moisture exchange
Semi-permeable membrane
Analytical and experimental validation

ABSTRACT

In Part I, a numerical model for coupled heat and moisture transfer in a run-around heat and moisture exchanger with a liquid desiccant coupling fluid is developed. The numerical model is two dimensional, transient and is formulated using the finite difference method with an implicit time discretization. The results from the numerical model for the case of only heat transfer for a single heat exchanger are compared to an available analytical solution and good agreement is obtained. For the simultaneous heat and moisture transfer in the run-around membrane energy exchanger (RAMEE), a comparison between numerical model results and experimental measurements obtained from laboratory testing for both sensible and latent effectiveness showed satisfactory agreement at different operating conditions. Part II of this paper applies the model for a range of initial conditions [32].

1. Introduction

The energy required to condition ventilation air typically constitutes 20–40% of the thermal load for commercial buildings [1] and can be even higher in educational buildings, hospitals and recreational facilities that require 100% fresh air to meet ventilation standards. This fact combined with the increasing cost of energy and environmental concerns has accelerated the demand for more efficient energy use in buildings. Air-to-air energy recovery in buildings has been shown to provide considerable energy savings and can decrease the required size of heating and cooling equipment by transferring heat and moisture between the supply side and the exhaust side of the ventilation system [2].

The existing air-to-air energy exchangers can be divided into two main groups: exchangers that transfer sensible heat only and exchangers that transfer both heat and moisture. In the past, air-to-air heat recovery systems, such as heat pipes [3] which are extensively used in many HVAC applications and aqueous-glycol run-around heat exchangers [4] have been designed to transfer only sensible heat. On the other hand, energy wheels which can transfer both heat and moisture between supply and exhaust airstreams in buildings have been studied for about two decades [5–7].

In recent years, extensive research has been performed on direct contact liquid desiccant systems because of their ability to effectively handle the latent energy or moisture loads of buildings. Park et al. [8] studied coupled heat and mass transfer between air and a triethylene glycol solution in a cross-flow configuration through a detailed numerical analysis. Ali et al. [9] evaluated the influence of the addition of Cu-ultrafine particles in the desiccant for the similar system. Mesquita et al. [10] developed a numerical model to analyze the combined heat and mass transfer in parallel flow (co-current and counter current) direct contact liquid-desiccant dehumidifiers considering variable thickness for desiccant film. Plate exchangers comprised of water permeable membrane exchange surface to transfer both heat and moisture have been proposed as an alternative to air-to-air energy recovery systems [11,12], but these require the supply and exhaust ducts to be located side-by-side.

A Run-Around Membrane Energy Exchanger (RAMEE), shown schematically in Fig. 1(a), has been suggested as a new system for energy recovery [13]. The RAMEE uses semi-permeable membranes in each exchanger with an aqueous salt solution coupling liquid pumped between the exchangers to transfer heat and water vapor simultaneously between the supply and exhaust airstreams [14]. Compared to rotary energy wheels, which recover both heat and moisture between adjacent ducts air flows, the RAMEE system may be more convenient to apply in retrofit applications where supply and exhaust ducts are remotely located. The only moving parts are liquid pumps and the run-around fluid. Carryover and cross-flow leakages of air, which are a concern for rotary wheels, should be negligible in the RAMEE system. The steady state performance of a RAMEE system has been simulated by Fan et al. [13], but there have been no research publications on the transient performance of run-around systems that transfer both heat and moisture between supply and exhaust airstreams. It is expected that these transient effects will be important during the operation of

* Corresponding author. Tel.: +1 306 966 5479; fax: +1 306 966 5427.
E-mail address: carey.simonson@usask.ca (C.J. Simonson).
[1] Ph.D. student at the University of Toronto.
[2] M.Sc. candidate at the University of Saskatchewan.
[3] Professor at the University of Saskatchewan.
[4] Professor Emeritus at the University of Saskatchewan.

0017-9310/$ - see front matter © 2009 Elsevier Ltd. All rights reserved.
doi:10.1016/j.ijheatmasstransfer.2009.07.012

Nomenclature

C	heat capacity rate [W/K]
C_{Salt}	concentration of salt solution (kg of salt per kg of solution) [%]
D_h	hydraulic diameter based on channel thickness [mm]
c_p	specific heat capacity [J/(kg K)]
d	channel thickness [mm]
H	enthalpy [J/kg]
h	convective heat transfer coefficient [W/(m^2 s)]
h_m	convective mass transfer coefficient [kg/(m^2 s)]
h_{fc}	net heat of phase change [J/kg]
k	thermal conductivity [W/(m K)]
k_m	moisture conductivity of membrane [kg/(m s)]
Le	Lewis number
M	mass [kg]
$\dot{m}$	mass flow rate [kg/s]
NTU	number of heat transfer units for each exchanger
NTU_m	number of mass transfer units for each exchanger
Nu	Nusselt number
P	total pressure [Pa]
Pe	Peclet number
p	partial pressure [Pa]
Q	pump volume flow rate [m^3/s]
q	heat loss/gain rate [W]
Re	Reynolds number
Sh	Sherwood number
T	temperature [K]
t	time [s]
t^*	dimensionless time defined relative to time required for the resident fluid to be replaced by the incoming fluid within a exchanger
U	overall heat transfer coefficient [W/(m^2 K)]
U_m	overall mass transfer coefficient [kg/(m^2 s)]
V	velocity [m/s]
W	humidity ratio [kg_v/kg_{Air}]
X	ratio of water mass to mass of pure salt [kg/kg]
x, y, z	coordinates
x_0, y_0, z_0	exchanger dimensions [m]
x^*, y^*	dimensionless coordinates

Greek symbols

α	dimensionless parameter which represents different dwell time for each fluid within a single heat exchanger
Δ	difference
ΔH_{Sol}	heat of solution [J/kg]
δ	thickness of membrane [mm]
ε	effectiveness
η	number of liquid desiccant circulation within both exchangers of a run-around system required to reach quasi-steady state condition
ρ_{Salt}	mass of salt [kg] per unit volume [m^3] of salt solution
ρ	density [kg/m^3]
θ	dimensionless temperature used for analytical/numerical comparison of a single heat exchanger
μ	initial ratio of mass of salt (or solution) in two exchangers to the total mass of salt (or solution) in the system
σ	heat loss/gain ratio which represents heat loss/gain rate relative to energy transfer rate within a exchanger
τ	dimensionless time of a run-around system defined relative to the transport time for the bulk solution to flow through both exchangers
τ^*	dimensionless time used for the analytical/numerical comparison of a single heat exchanger
ψ, ω	general properties

Subscripts

Air	air side
E	exhaust side
ex	exchanger
f	fluid
g	moist air
Indoor	indoor condition
in	inlet
l	latent
out	outlet
S	supply side
Salt	pure salt
Sol	salt solution
s	sensible
st	storage tank
v	water vapor

these systems because the thermal and mass capacity of the liquid is large compared to that for the air.

The objective of Part I of this paper is to develop and verify a theoretical/numerical model with a finite difference formulation to investigate the transient performance of a run-around system for exchanging heat and moisture between two airstream using two cross-flow flat plate heat exchangers, one in each airstream at different operating conditions. The accuracy of the numerical model is verified for the case of no moisture transfer with an available analytical heat transfer solution [15] and for the case of simultaneous heat and moisture transfer with experimental data [16] from laboratory testing of a RAMEE system. The verified numerical model will help to investigate the behavior of the system under different operating conditions.

2. Mathematical formulation

A run-around membrane energy exchanger (RAMEE) system is comprised of two liquid-to-air membrane energy exchangers (LAMEE), two storage tanks, connecting tubing and pumps as shown in Fig. 1(a). Each LAMEE has multiple air and liquid flow channels each separated by a semi-permeable membrane. The geometry of one pair of flow channels for a cross-flow flat plate LAMEE and the coordinate system used for the mathematical model are shown in Fig. 1(b). Here the salt solution flows vertically through the exchanger in the positive y-direction and air flows horizontally through the exchanger in the positive x-direction. In this exchanger, the semi-permeable membranes allow water vapor to diffuse normal to the plane of the membrane (in the z-direction) and the air and desiccant streams transport this water vapor and heat downstream (in the positive x and y-directions). Liquid water is prevented from entering the air channels by the membrane [14].

2.1. Assumptions

The following assumptions are made for the mathematical analysis:

(1) In order to model heat and mass transfer, the bulk mean temperatures and moisture concentrations of each fluid flow within a channel are used. These flows are assumed to be laminar and fully developed (i.e., entrance effects are negligible).

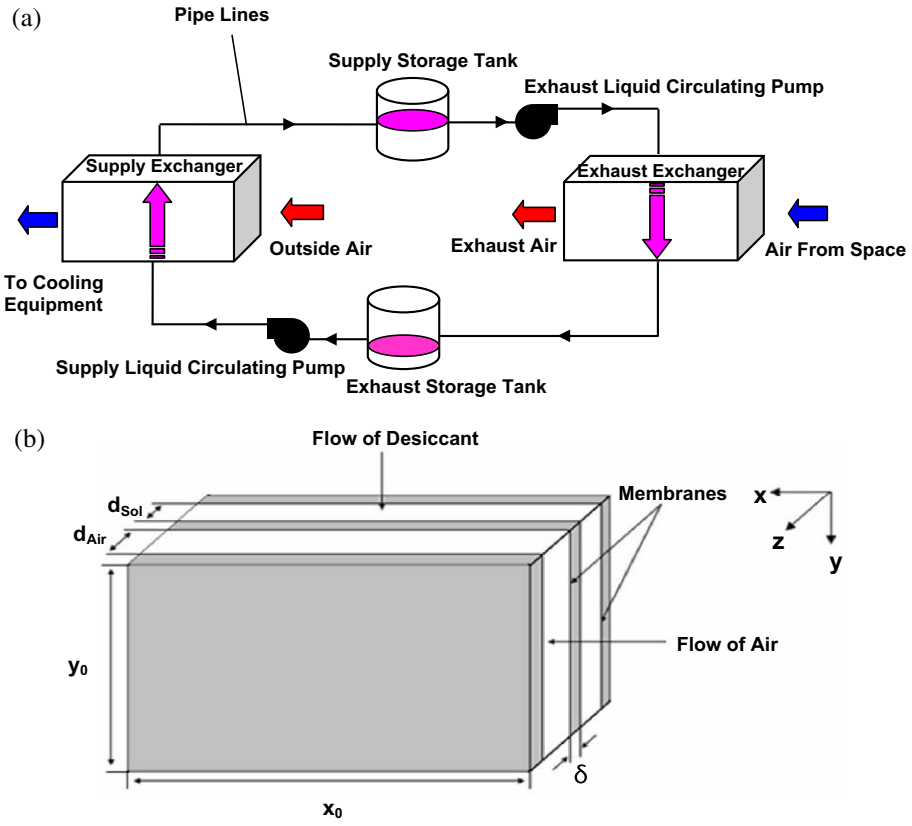

Fig. 1. (a) Schematic of the run-around membrane energy exchanger (RAMEE) system and (b) schematic of cross-flow liquid-to-air membrane energy exchanger (LAMEE).

(2) The heat and mass transfer processes occur only normal to each membrane in the z-direction and the membrane properties are constant.
(3) Axial heat conduction and water vapor molecular diffusion in the two fluids in the flow directions are negligible. The water vapor diffusion resistance of the salt solution in the transverse direction (z-direction) is negligible compared to the resistance of the membrane and air flow boundary layer.
(4) Heat gain or loss due to adsorption/desorption of water vapor at the membrane surface occurs only in the liquid component.
(5) The membrane thermal and mass transfer capacitance effects are negligible.
(6) The desiccant liquid in the storage tanks is well mixed at all times.

The first assumption avoids the problem of determining the lateral temperature and moisture concentration distributions in each channel and simplifies the problem to one dimensional for the bulk fluid variables. Entrance effects will be negligible for these exchangers because the inverse heat and mass transfer Graetz numbers are greater than 0.05, resulting in constant heat and mass transfer coefficients [17]. It is observed that the entrance regions of the air and the liquid desiccant flows are less than 6% of the exchanger length in the pertinent direction for typical operating conditions. Therefore, in practical operating conditions, the effect of entry length will be negligible. As well, the Reynolds numbers for both fluids in the exchanger remain in the laminar flow range for most operating conditions.

The second assumption is valid because the membrane is thin and has a higher thermal and moisture transfer resistance compared to convective heat and mass transfer resistance, respectively. As well, the surface area to volume ratio for the exchanger is high. Therefore, one dimensional diffusion through the semi-permeable membrane occurs normal to each surface. Assumption 3 arises because Pe is greater than 20 in most of the operating conditions in this study. The effect of axial dispersion is generally neglected for $Pe > 20$ [18] and is quite small even for $Pe > 10$ [19]. The diffusion resistance of the solution in the z-direction is neglected because simulations show that including the resistance to moisture transfer in the solution changes the effectiveness values by less than 0.01 for the cases in this paper.

The energy of phase change is assumed to be delivered to or obtained from the liquid desiccant [20] in Assumption 4, because the convective heat and mass transfer coefficients on the air side are typically an order of magnitude smaller than the convective heat and mass transfer coefficients on the liquid side. In addition, the phase change between the liquid and vapor states occurs at the interface between the liquid and the membrane. The fifth assumption simplifies the analysis; however, it is valid since the membrane has negligible thermal capacity and mass compared to thermal and mass transfer capacitance of desiccant fluid in the system [21]. Assumption 6 implies that the outlet properties of the salt solution in the storage tanks are the same as the average reservoir content at any time due to fluid mixing.

2.2. Analysis of a cross-flow channel between air and solution (LAMEE)

Based on the above assumptions, the governing equations for the coupled heat and moisture transfer through the permeable membrane in a LAMEE are now presented. The set of governing equations at any point (x, y) on the membrane surface consist of one pair of heat and moisture transfer equations for the air side and another pair for the liquid side.

The change of water vapor content with time at any point (x, y) in the air side within the exchanger is determined by knowing

mass gain/loss in the air flowing in the x-direction and water vapor flux through the membrane in the z-direction:

$$\rho_{\mathrm{Air}} d_{\mathrm{Air}} \frac{\partial W_{\mathrm{Air}}}{\partial t} + \frac{\dot{m}_{\mathrm{Air}}}{y_0} \frac{\partial W_{\mathrm{Air}}}{\partial x} + 2U_{\mathrm{m}}(W_{\mathrm{Air}} - W_{\mathrm{Sol}}) = 0, \tag{1}$$

where $\dot{m}_{\mathrm{Air}}$ is the mass flow rate of dry air through a single channel, W_{Air} is the bulk humidity ratio of the air and W_{Sol} is the humidity ratio of the air that is in equilibrium with the salt solution at the interface between the solution and the membrane. Since the resistance to moisture transfer in the solution is very small, it is assumed that the concentration of the solution is uniform in the z-direction and equal to the bulk concentration. Therefore, the equilibrium humidity ratio of salt solution (W_{Sol}) depends on the bulk temperature and concentration of the salt solution:

$$W_{\mathrm{Sol}} = f(X_{\mathrm{Sol}}, T_{\mathrm{Sol}}). \tag{2}$$

In order to calculate this property, the analytical expression is used as presented in Ref. [22]. The symbol d_{Air} is the air channel thickness and, y_0 is the exchanger length along desiccant flow direction, and the symbol U_{m} is the overall mass transfer coefficient for water vapor flux between the air and salt solution and is defined as:

$$U_{\mathrm{m}} = \left[\frac{\delta}{k_{\mathrm{m}}} + \frac{1}{h_{\mathrm{m,Air}}}\right]^{-1}. \tag{3}$$

In the above equation, the convective mass transfer coefficient between the membrane and the airstream ($h_{\mathrm{m,Air}}$) is assumed to be constant for any operating conditions. Similarly the water vapor permeability (k_{m}) of the membrane is assumed to be constant because k_{m} is a weak function of temperature and humidity [14]. Since the thickness of the membrane (δ) is constant, U_{m} is not a function of the position within the exchanger.

The energy equation for the air side at any point (x, y) includes energy storage, convection and energy transfer through the membrane and is:

$$\rho_{\mathrm{g}} c_{p_{\mathrm{g}}} d_{\mathrm{Air}} \frac{\partial T_{\mathrm{Air}}}{\partial t} + \frac{\dot{m}_{\mathrm{Air}}}{y_0} c_{p_{\mathrm{g}}} \frac{\partial T_{\mathrm{Air}}}{\partial x} + 2U(T_{\mathrm{Air}} - T_{\mathrm{Sol}}) = 0, \tag{4}$$

where T_{Air} is the bulk mean temperature of the air, ρ_{g} the density of moist air, and $c_{p_{\mathrm{g}}}$ is the thermal capacity of moist air defined as:

$$c_{p_{\mathrm{g}}} = \frac{c_{p_{\mathrm{Air}}} + W_{\mathrm{Air}} c_{p_{\mathrm{v}}}}{1 + W_{\mathrm{Air}}}, \tag{5}$$

and U is the overall heat transfer coefficient between the air and salt solution and can be expressed as follows:

$$U = \left[\frac{1}{h_{\mathrm{Sol}}} + \frac{\delta}{k} + \frac{1}{h_{\mathrm{Air}}}\right]^{-1}. \tag{6}$$

At any point (x, y) in the liquid desiccant side within exchanger, the change of moisture content (X_{Sol}) with time can be determined by knowing the mass gain/loss in the liquid flowing in the y-direction and water vapor flux through the membrane:

$$\rho_{\mathrm{Salt}} d_{\mathrm{Sol}} \frac{\partial X_{\mathrm{Sol}}}{\partial t} + \frac{\dot{m}_{\mathrm{Salt}}}{x_0} \frac{\partial X_{\mathrm{Sol}}}{\partial y} - 2U_{\mathrm{m}}(W_{\mathrm{Air}} - W_{\mathrm{Sol}}) = 0, \tag{7}$$

where $\dot{m}_{\mathrm{Salt}}$ is the mass flow rate of dry salt through a single channel, ρ_{Salt} is the amount of salt (kg) volume (m^3) of salt solution and X_{Sol} is defined as:

$$X_{\mathrm{Sol}} = \frac{\text{mass of water}}{\text{mass of salt}}. \tag{8}$$

W_{Sol} is obtained from the equation of state [Eq. (2)], at equilibrium for the salt solution knowing X_{Sol} and T_{Sol} [22].

The energy equation for the liquid side any point (x, y) includes energy storage, convection, the heat of phase change and energy transfer through the membrane and can be expressed as:

$$\rho_{\mathrm{Sol}} c_{p_{\mathrm{Sol}}} d_{\mathrm{Sol}} \frac{\partial T_{\mathrm{Sol}}}{\partial t} + \frac{\dot{m}_{\mathrm{Sol}}}{x_0} c_{p_{\mathrm{Sol}}} \frac{\partial T_{\mathrm{Sol}}}{\partial y} - 2U_{\mathrm{m}}(W_{\mathrm{Air}} - W_{\mathrm{Sol}}) h_{\mathrm{fc}} - 2U(T_{\mathrm{Air}} - T_{\mathrm{Sol}}) = 0, \tag{9}$$

where T_{Sol} is the bulk mean temperature of salt solution, ρ_{Sol} the bulk mean density of salt solution, h_{fc} is the net heat of phase change which includes the heat of vaporization of water and the heat of solution and $c_{p_{\mathrm{Sol}}}$ is the specific heat capacity of salt solution as a function of temperature and concentration. The analytical expressions presented in Ref. [23] are used for the salt solution properties.

2.2.1. Normalization of equations

The method of deriving the governing dimensionless heat and moisture transfer groups for this study from the governing equations follows the method presented by Shah [24] and Romie [15]. These dimensionless groups are the number of heat transfer units NTU, the number of mass transfer units $\mathrm{NTU_m}$ and dimensionless times based on the times required for the resident fluids to be replaced by the incoming fluids in the exchanger. The set of equations are as follows:

Air side:

$$\frac{\partial W_{\mathrm{Air}}}{\partial t^*_{\mathrm{Air}}} + \frac{\partial W_{\mathrm{Air}}}{\partial x^*} + \mathrm{NTU_{m,Air}}(W_{\mathrm{Air}} - W_{\mathrm{Sol}}) = 0, \tag{10}$$

$$\frac{\partial T_{\mathrm{Air}}}{\partial t^*_{\mathrm{Air}}} + \frac{\partial T_{\mathrm{Air}}}{\partial x^*} + \mathrm{NTU_{Air}}(T_{\mathrm{Air}} - T_{\mathrm{Sol}}) = 0. \tag{11}$$

Liquid Side:

$$\frac{\partial X_{\mathrm{Sol}}}{\partial t^*_{\mathrm{Sol}}} + \frac{\partial X_{\mathrm{Sol}}}{\partial y^*} - \mathrm{NTU_{m,Sol}}(W_{\mathrm{Air}} - W_{\mathrm{Sol}}) = 0, \tag{12}$$

$$\frac{\partial T_{\mathrm{Sol}}}{\partial t^*_{\mathrm{Sol}}} + \frac{\partial T_{\mathrm{Sol}}}{\partial y^*} - \mathrm{NTU_{Sol}}(T_{\mathrm{Air}} - T_{\mathrm{Sol}}) - \frac{\mathrm{NTU_{m,Sol}}}{c_{p_{\mathrm{Sol}}}(1 + X_{\mathrm{Sol}})} h_{\mathrm{fc}}(W_{\mathrm{Air}} - W_{\mathrm{Sol}}) = 0. \tag{13}$$

where

$$x^* = \frac{x}{x_0}, \tag{14}$$

$$y^* = \frac{y}{y_0}, \tag{15}$$

$$t^*_{\mathrm{Air}} = \frac{tV_{\mathrm{Air}}}{x_0} \tag{16}$$

$$t^*_{\mathrm{Sol}} = \frac{tV_{\mathrm{Sol}}}{y_0}, \tag{17}$$

and

$$\mathrm{NTU_{Air}} = \frac{2Ux_0y_0}{C_{\mathrm{g}}}, \tag{18}$$

where

$$C_{\mathrm{g}} = \dot{m}_{\mathrm{Air}}(c_{p_{\mathrm{Air}}} + c_{p_{\mathrm{v}}} W_{\mathrm{Air}}). \tag{19}$$

Also,

$$\mathrm{NTU_{Sol}} = \frac{2Ux_0y_0}{C_{\mathrm{Sol}}} \tag{20}$$

where the number of heat transfer units for a LAMEE is defined as:

$$\mathrm{NTU} = \max\{\mathrm{NTU_{Air}}, \mathrm{NTU_{Sol}}\}. \tag{21}$$

Finally,

$$\mathrm{NTU_{m,Air}} = \frac{2U_{\mathrm{m}}x_0y_0}{\dot{m}_{Air}}, \tag{22}$$

and

$$NTU_{m,Sol} = \frac{2U_m x_0 y_0}{\dot{m}_{Salt}}. \quad (23)$$

where the number of mass transfer units for a LAMEE is defined as:

$$NTU_m = \max\{NTU_{m,Air}, NTU_{m,Sol}\} \quad (24)$$

2.2.2. Boundary and initial conditions

The initial temperature of the salt solution and the air are assumed to be equal to indoor temperature:

$$T_{Air}(x^*, y^*, 0) = T_{Sol}(x^*, y^*, 0) = T_{Indoor}. \quad (25)$$

Eq. (25) indicates that the initial conditions of both exchangers are equal to the temperature representative of the exhaust air conditions. This assumption is due to the fact that the entire system is assumed to be located in a mechanical room that has conditions similar to the indoor air in the building. Thus, before the step change in the supply air, the air streams are assumed to be in equilibrium with indoor condition which has the same temperature as the exhaust side airstream.

The inlet temperature of the air on the supply side ($T_{Air,S}$) is assumed to be subjected to a finite step change at time zero:

$$T_{Air,S}(0, y^*, \tau) = T_{Air,in,S}, \quad (26)$$

while the inlet temperature of the exhaust air ($T_{Air,E}$) is assumed to be constant throughout the simulation:

$$T_{Air,E}(0, y^*, \tau) = T_{Indoor}. \quad (27)$$

A characteristic dimensionless time (τ) for the RAMEE system is defined relative to the transport time for the bulk solution to flow through both exchangers without considering the storage tanks or connecting tubes:

$$\tau = \frac{1}{{t^*_{Sol,S}}^{-1} + {t^{*-1}_{Sol,E}}^{-1}}, \quad (28)$$

τ indicates the number of complete volume circulations of the salt solution in both exchangers. This dimensionless number is a function of both the liquid desiccant volume flow rate and the length of exchangers in the direction of salt solution flow. This parameter is used to interpret the transient response of the system at different operating conditions.

The initial humidity ratio of the air is equal to the indoor air humidity ratio (similar to the assumption of the initial air temperature);

$$W_{Air}(x^*, y^*, 0) = W_{Air,Indoor}. \quad (29)$$

Similar to the temperature boundary conditions, the air humidity ratio in the supply side is subjected to a finite step change at time 0:

$$W_{Air,S}(0, y^*, \tau) = W_{Air,in,S}, \quad (30)$$

while the inlet humidity ratio of the exhaust air remains unchanged as

Table 1
AHRI air conditions used as the inlet condition of the supply and exhaust exchangers (LAMEEs) in the run-around system (RAMEE).

Summer	$T_{Air,in,S}$	308.15 K (35 °C)
	$W_{Air,in,S}$	17.5 g/kg
	$T_{Air,in,E}$	297.15 K (24 °C)
	$W_{Air,in,E}$	9.3 g/kg
Winter	$T_{Air,in,S}$	274.85 K (1.7 °C)
	$W_{Air,in,S}$	3.5 g/kg
	$T_{Air,in,E}$	294.15 K (21 °C)
	$W_{Air,in,E}$	7.1 g/kg

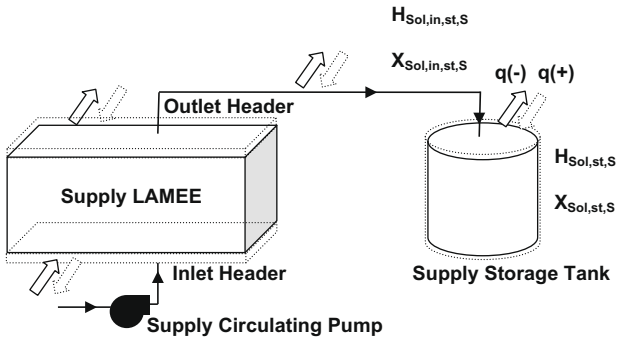

Fig. 2. Schematic of a storage tank and a LAMEE showing the concentrations and enthalpies for the supply sub-system as a control volume.

$$W_{Air,E}(0, y^*, \tau) = W_{Air,Indoor}. \quad (31)$$

AHRI summer and winter test conditions [25] are used as the air inlet condition of the run-around system as shown in Table 1. The AHRI test conditions are defined to be representative of typical summer and winter operating conditions in many climates. Inlet temperatures below 0 °C are not included.

In practical situations the initial concentration of the salt solution could be selected as an arbitrary single value so that:

$$X_{Sol}(x^*, y^*, 0) = X_{Sol,Initial}. \quad (32)$$

The influence of this initial concentration on the system behavior will be discussed in detail later. The difference between the initial concentration and the concentration of the liquid desiccant at steady state condition can be defined as follows:

$$\Delta C_{Salt} = C_{Salt,Initial} - C_{Salt,Steady\ State}. \quad (33)$$

However, ΔC_{Salt} is considered to be zero in this study unless otherwise indicated.

2.3. Analysis of mixing process in the storage tanks

In the RAMEE system, the liquid desiccant that leaves an exchanger will mix with salt solution stored in the next reservoir as shown in Fig. 2. Then, this salt solution will be pumped to the other exchanger to be circulated in the system. Therefore, the preceding storage tank conditions are used as inlet salt solution conditions for the LAMEEs within the run-around system. The inlet liquid desiccant conditions for the supply exchanger are:

$$T_{Sol,in,ex,S}(x^*, 0, \tau) = T_{Sol,st,E}(\tau), \quad (34)$$

$$X_{Sol,in,ex,S}(x^*, 0, \tau) = X_{Sol,st,E}(\tau). \quad (35)$$

As well, for the exhaust exchanger the inlet (boundary) conditions of salt solution are given by the following equations:

$$T_{Sol,in,ex,E}(x^*, 0, \tau) = T_{Sol,st,S}(\tau), \quad (36)$$

$$X_{Sol,in,ex,E}(x^*, 0, \tau) = X_{Sol,st,S}(\tau). \quad (37)$$

The above equations which reflect the effect of pumps, piping and storage tanks couple two LAMEEs to form a RAMEE.

To determine the conditions of the solution in the storage tanks, the set of governing equations for the storage tanks can be developed using Assumption 6 and the constant mass of salt in the system. In order to develop the equations describing the conservation of mass and energy, one exchanger with a storage tank is considered as one control volume and a sub-system as shown in Fig. 2. The exhaust sub-system, which is not shown, is similar to supply sub-system with a similar exchanger, storage tank and circulating pump.

The principle of conservation of mass for water in the supply storage tank gives:

$$\frac{d}{dt}(M_{Salt,st,S}X_{Sol,st,S}) = \dot{m}_{Salt,in,st,S}X_{Sol,in,st,S} - \dot{m}_{Salt,out,st,S}X_{Sol,st,S}, \quad (38)$$

where $M_{Salt,st,S}$ is the mass of salt in the supply storage tank and varies during the transient period. This value can be calculated from the principle of conservation of mass for pure salt in the supply storage tank as follows:

$$\frac{d}{dt}(M_{Salt,st,S}) = \dot{m}_{Salt,in,st,S} - \dot{m}_{Salt,out,st,S}. \quad (39)$$

The mass flow rate of salt which enters the supply storage tank is calculated from the volume flow rate of the pump in the supply sub-system and the concentration of the salt solution that exists the supply exchanger.

$$\dot{m}_{Salt,st,in,S} = \frac{\rho_{Sol,out,ex,S}Q_S}{1 + X_{Sol,out,ex,S}}, \quad (40)$$

where Q_S is the supply circulating pump volume flow rate and $\rho_{Sol,out,ex,S}$ is the density of desiccant fluid as it exits from the supply exchanger. The density of the salt solution is a function of its temperature and concentration. This correlation is given in Ref. [23]. It should be reminded that the salt solution in each tank is assumed to be well mixed.

The mass flow rate of the salt leaving the supply storage tank and delivered to the exhaust exchanger is calculated using an equation similar to Eq. (40):

$$\dot{m}_{Salt,st,out,S} = \frac{\rho_{Sol,st,S}Q_E}{1 + X_{Sol,st,S}} \quad (41)$$

where Q_E is the volume flow rate of the exhaust pump.

In order to calculate the temperature of the desiccant in the storage tank at any time, the conservation of energy, including the heat of solution [26], is required and is presented in a similar form to Eq. (39),

$$\begin{aligned}&\frac{d}{dt}[M_{Sol,st,S}(C_{Salt,st,S}\Delta H_{Sol,st,S}(T_0) + c_{p_{Sol,st,S}}(T_{Sol,st,S} - T_0))]\\ &= \dot{m}_{Sol,in,st,S}[C_{Salt,in,st,S}\Delta H_{Sol,in,st,S}(T_0) + c_{p_{Sol,in,st,S}}(T_{Sol,in,st,S} - T_0)]\\ &\quad - \dot{m}_{Sol,out,st,S}[C_{Salt,st,S}\Delta H_{Sol,st,S}(T_0) + c_{p_{Sol,st,S}}(T_{Sol,st,S} - T_0)] + q, \end{aligned} \quad (42)$$

where C_{Salt} is defined as:

$$C_{Salt} = \frac{1}{1 + X_{Sol}}. \quad (43)$$

T_0 is the reference temperature and ΔH_{Sol}, which depends on salt solution concentration, is the heat of solution per kilogram of salt at temperature T_0 [23]. The mass of solution in the storage tank and the mass flow rate of salt solution used in the conservation of energy equation are, respectively equal to:

$$M_{Sol} = M_{Salt}(1 + X_{Sol}) \quad (44)$$

$$\dot{m}_{Sol} = \dot{m}_{Salt}(1 + X_{Sol}). \quad (45)$$

In Eq. (42), q accounts for heat gain to or loss from the salt solution as it flows from the outlet of the supply exchanger to the inlet of the exhaust exchanger as shown schematically in Fig. 2. Therefore it accounts for heat gain/loss in: (i) the outlet header of the supply exchanger, (ii) the inlet header of the exhaust exchanger, (iii) the supply storage tank, (iv) the piping connecting the outlet of the supply exchanger and the inlet of the exhaust exchanger due to temperature differences between the fluid and the surroundings and (v) the energy that pump adds to the liquid desiccant circuit. In order to introduce the value of heat loss/gain into the system as dimensionless parameter, the heat loss/gain coefficient σ is defined as below for supply and exhaust sides of the RAMEE system separately as follows:

$$\sigma = \frac{q_{loss/gain}}{|C_{Sol,out,ex}T_{Sol,out,ex} - C_{Sol,in,ex}T_{Sol,in,ex}|}, \quad (46)$$

where C_{Sol} is the heat capacity rate of salt solution. Heat loss from the system results in a negative value of σ, while heat gain to the system results in a positive coefficient.

The salt solution properties [i.e., temperature (T) and water mass fraction (X_{Sol})] within storage tanks are the properties that couple two LAMEEs in the run-around system and should be calculated to investigate the behavior of the system. It is also important to analyze the changes in liquid levels in the storage tanks as the operating conditions change because the volume of water in the system will be low during dry conditions (winter) and high during humid conditions (summer). This analysis of the storage tanks and their maximum volume change are critical to provide design guidance for the selection of the appropriate storage volume of the liquid desiccant in the system for the full range of operating conditions over a typical day, month or year. With storage tanks in the mathematical/numerical model, the question of how the thermal and mass capacitances of the desiccant fluid in the storage tanks are related to the transient response time of the system can be addressed. In order to answer this question a new dimensionless parameter is defined. This parameter is the ratio of the mass of salt in the exchangers to the total mass of salt in the RAMEE system (including exchanger, headers, piping and storage tanks) and is called the mass ratio (μ) and is expressed as:

$$0 < \mu = \frac{\text{Mass of salt in the exchangers}}{\text{Total mass of salt in the system}} < 1. \quad (47)$$

During a transient simulation, the mass ratio (μ) will change as the concentration of the solution and volume of water in the system change and the value reported will be the value that exists at the initial conditions.

2.4. Overall heat and mass transfer coefficients

Magnesium chloride aqueous salt solution is chosen as the coupling fluid in this study. In order to calculate the overall heat and mass transfer coefficients in Eqs. (3) and (6), the convection coefficients (h and h_m), the membrane conductivities (k and k_m) and the thickness of membrane (δ) are required. For fully developed laminar flow [27] with $Re \leqslant 2300$, the dimensionless heat transfer coefficient (Nu) is independent of Re:

$$Nu = \text{constant} = \frac{hD_h}{k_f}, \quad (48)$$

where D_h is the hydraulic diameter of the flow channel. For parallel plates, D_h is the twice the channel spacing. In this study Nu = 8.24 [27], which is the case for fully developed convective heat transfer between infinite rectangular plates with uniform heat flux, is selected.

Table 2
Selected design parameters of the LAMEE.

Name	Symbol	Value
Size of exchanger	$x_0 \times y_0 \times z_0$	$0.6 \times 0.3 \times 0.076$ m
Channel thickness, air side	d_A	4.9 mm
Channel thickness, liquid side	d_L	1.7 mm
Number of air channels	n_A	10
Number of liquid channels	n_L	10
Membrane thickness	δ	0.5 mm
Thermal conductivity of membrane	k	0.3 W/(m K)
Moisture conductivity of membrane	k_m	1.66×10^{-6} kg/(m s)

The Chilton-Colburn Analogy [28] is used to determine the dimensionless convective mass transfer coefficient (Sh) from Nu and Lewis number (Le),

$$Sh = NuLe^{-2/3}, \tag{49}$$

or the mass transfer coefficient can be calculated as:

$$h_m = \frac{h}{c_p} Le^{-2/3}. \tag{50}$$

The heat and mass conductivities (k and k_m) of the semi-permeable membrane depend on the membrane type and are needed to calculate the overall heat and mass transfer coefficients (U). Polypropylene (PP) which is a polymer that is common in many household applications such as microwave tolerant plastics and indoor/outdoor carpeting is used as the semi-permeable membrane in this study. The thermal and moisture conductivities of the membrane used in this study are $k = 0.3$ W/(m K) and $k_m = 1.66 \times 10^{-6}$ kg/(m s) [14]. The thickness of membrane is 0.5 mm. These values and the other parameters for the liquid to air membrane energy exchanger (LAMEE) studied in this research are listed in Table 2.

2.5. Properties of $MgCl_2$ solution

Empirical property correlations, which are valid for the range $273.15 \leqslant T \leqslant 373.15$ K, are used to calculate the properties of $MgCl_2$ solution. These correlations are given in Refs. [22] and [23].

To determine the equilibrium humidity ratio of the air adjacent to the solution, the partial pressure of the water vapor, p_v, and the total pressure, P, of an air mixture are used as follows:[1]

$$W_{Sol} = 0.62198 \frac{p_v}{P - p_v}. \tag{51}$$

In this study, correlations developed by Cisternas and Lam [22] for the equilibrium water vapor pressure of aqueous solutions are used to calculate the equilibrium water vapor pressure at any temperature and salt solution concentration. The reported average deviation between these correlations and experimental data for $MgCl_2$ salt solution with concentrations less than 27.6% by weight is 0.9% [22]. The same correlations are used to extrapolate from 27.6% salt solution concentration to saturation concentration (35.9%) in this paper. Using the correlation for the equilibrium water vapor pressure of aqueous $MgCl_2$ in conjunction with Eq. (51), the equilibrium concentration lines for the $MgCl_2$ can be obtained. Fig. 3 shows the equilibrium concentration lines superimposed on the psychrometric chart, where C_{Salt} is the salt concentration at equilibrium and defined in Eq. (43).

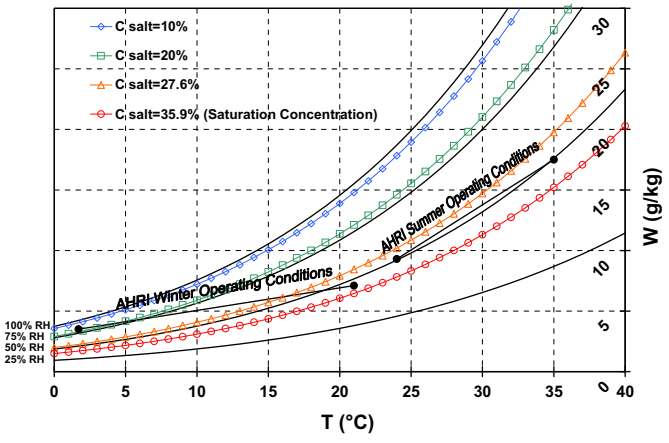

Fig. 3. Equilibrium constant concentration lines of an $MgCl_2$ solution superimposed on the psychrometric chart.

As it can be seen in Fig. 3, the equilibrium constant concentration lines of the salt solution nearly follow the same trend as the constant relative humidity lines when superimposed on the psychrometric chart. Fig. 3 also shows the magnesium chloride saturation concentration as a limit for salt solution properties calculations. As illustrated in Fig. 3, during AHRI winter operating conditions the salt solution will be quite close to saturation conditions when the salt solution is in equilibrium with the indoor air conditions. If saturation conditions exist in a LAMEE, salt crystals could deposit on the membrane surface and alter the heat and moisture transfer characteristics of the semi-permeable membrane [29,30]. As well, solid particles of salt could block the desiccant flow passages and cause pump problems. Therefore, the risk of crystallization of the salt solution must be considered in the numerical model as a constraint or limit because the heat and mass transfer equations used in the simulation are only valid for the case of no salt crystallization. Also, in practical situations, the system should avoid operating conditions where the solution has a concentration close to the saturation concentration in order to avoid the previously mentioned problems. In the current study the crystallization of salt solution is not considered and only conditions where crystallization does not occur are studied.

2.6. Method of solution

The governing equations for each exchanger are discretised using the implicit finite difference technique for the time derivative and the upwind scheme for the first order spatial derivative. The discretised equations along with the initial and boundary conditions are solved using the Gauss–Seidal iteration technique. The convergence of the solution has been checked by varying the number of spatial grids and time steps. Simulation results show that a spatial grid of 100×100 for the exchanger with properties mentioned in Table 2 along with time steps ($\Delta\tau$) of 1/9 give an grid independent solution. For example, increasing the number of spatial grids from 100×100 to 140×140 and decreasing the time step from 1/9 to 1/45, changes the predicted effectiveness values of the RAMEE system during transient time by less than 0.002, but increases the solution time by a factor of 3. A trial and error method is employed in the well mixed reservoirs to find the time dependent salt solution properties in each storage tank from energy and mass balances equations. The solution gives two dimensional temperature and humidity ratio distributions within both the air and salt solution throughout the exchangers as a function of time. Additionally, one may calculate the outlet bulk mean temperatures of the air and liquid desiccant for the LAMEE by the following equations:

$$T_{Air,out} = \frac{1}{\dot{m}_{Air} c_{p_{Air}} y_0} \int_y \dot{m}_A c_{p_{Air}} T_{Air}\, dy, \tag{52}$$

$$T_{Sol,out} = \frac{1}{\dot{m}_{Sol} c_{p_{Sol}} x_0} \int_x \dot{m}_{Sol} c_{p_{Sol}} T_{Sol}\, dx, \tag{53}$$

As well, the outlet bulk mean water contents of the air and the salt solution fluid are calculated as follows:

$$W_{Air,out} = \frac{1}{y_0} \int_y W_{Air}\, dy, \tag{54}$$

$$X_{Sol,out} = \frac{1}{x_0} \int_x X_{Sol}\, dx. \tag{55}$$

2.7. Effectiveness of the RAMEE system

In order to investigate the effect of various parameters on the heat and moisture transfer rates in the run-around system during the transient period, dimensionless numbers (i.e., effectiveness

values) are used. These effectiveness values relate the heat and moisture transfer rates at any time relative to the maximum possible heat and moisture transfer rates for the exchangers based on the specific operating conditions. With known air inlet conditions, the sensible effectiveness or dimensionless heat transfer rate at any time (τ) with equal mass flow rates of air for the supply side exchanger is defined as:

$$\varepsilon_{s,S}(\tau) = \frac{T_{Air,in,S} - T_{Air,out,S}}{T_{Air,in,S} - T_{Air,in,E}}, \tag{56}$$

and for the exhaust side exchanger is,

$$\varepsilon_{s,E}(\tau) = \frac{T_{Air,out,E} - T_{Air,in,E}}{T_{Air,in,S} - T_{Air,in,E}}. \tag{57}$$

It can be seen in the above equations that the air side properties are used to calculate the effectiveness in this study because the changes in the air properties can be measured more easily and with lower uncertainties than the changes in the salt solution properties. This allows the results from the numerical model to be compared with experimental measurements. Besides, in practical HVAC applications, the air properties and their changes are the most important parameters for the performance of the HVAC system. Using the same form of equations, the latent effectiveness or dimensionless moisture transfer rate for the supply and exhaust side exchangers are, respectively:

$$\varepsilon_{l,S}(\tau) = \frac{W_{Air,in,S} - W_{Air,out,S}}{W_{Air,in,S} - W_{Air,in,E}} \tag{58}$$

$$\varepsilon_{l,E}(\tau) = \frac{W_{Air,out,E} - W_{Air,in,E}}{W_{Air,in,S} - W_{Air,in,E}}. \tag{59}$$

It is important to note that for the case of no external heat gain/loss from/to the surroundings, the system energy and mass balances ensure that the dimensionless heat and moisture transfer rates in the supply side exchanger become the same as those in the exhaust side exchanger and equal to the steady state effectiveness as the run-around energy recovery system moves toward equilibrium.

2.8. Quasi-steady state

In order to investigate the transient behaviour of the system, the performance of the RAMEE system is studied for a sufficient time duration so that quasi-steady state is obtained for each operating condition. In this study, the number of circulations needed to reach quasi-steady state is given the symbol η. In other words, when $\tau \geqslant \eta$, the RAMEE system is operating in quasi-steady state condition. Two different sets of criteria are adopted to define quasi-steady state conditions for different initial salt solution concentrations.

The first definition is based on energy and mass balances of the airstreams and is applied for the case of $\Delta C_{Salt} = 0$ in Eq. (33). For this initial condition, quasi-steady state is defined as the time when all the energy and moisture that is lost by one airstream is taken up by the other airstream. This exists, for balanced air flow rates, when:

$$\left|\frac{(W_{Air,in,S} - W_{Air,out,S}) - (W_{Air,out,E} - W_{Air,in,E})}{(W_{Air,in,S} - W_{Air,in,E})}\right| \leq 1 \times 10^{-2}, \tag{60}$$

and,

$$\left|\frac{(H_{Air,in,S} - H_{Air,out,S}) - (H_{Air,out,E} - H_{Air,in,E})}{(H_{Air,in,S} - H_{Air,in,E})}\right| \leq 1 \times 10^{-2}. \tag{61}$$

If the quasi-steady convergence criteria are set to 5×10^{-3}, the quasi steady effectiveness values (i.e., sensible, latent and total effectivenesses) change by less than 0.003 from those predicted with convergence criteria of 1×10^{-2}, indicating that the convergence limits in Eqs. (60) and (61) are satisfactory. It needs to be mentioned that in presence of external heat loss/gain from/to the RAMEE system, Eq. (61) is modified to account for the impact of those losses or gains on the energy balance of the system and set as the quasi-steady state criterion in this case.

When the initial salt solution concentration is different from the steady state value (i.e., $\Delta C_{Salt} \neq 0$), the time required to satisfy the energy and mass balances is very large. This is observed from both simulation (see Part II) and experimental results as will be discussed in detail later. Due to this very slow transient response of the RAMEE system for the case of $\Delta C_{Salt} \neq 0$, substantial computational resources are required to reach quasi-steady state as defined by the energy and mass balances. As a result, a second quasi-steady state convergence criterion is proposed as follows:

$$\left|\frac{\partial \varepsilon}{\partial \tau}\right| \leq 5 \times 10^{-6}. \tag{62}$$

This above criterion illustrates that quasi-steady state is achieved where the rate of change in the effectiveness values of the RAMEE system is less than a certain value during the transient period. Simulation results show that decreasing this value from the selected value of 5×10^{-6} to 1×10^{-6} changes the predicted individual effectiveness values (e.g., supply latent effectiveness) by less than 0.017, while the average effectiveness (i.e., the average of supply and exhaust) values change only by less than 0.0005. The implication is that the average effectivenesses reach their quasi-steady state values much quicker than the individual exchanger effectiveness and can be predicted by proposed quasi-steady convergence criterion satisfactorily. Due to aforementioned decreasing in the right hand side of Eq. (62), the number of circulations of the liquid desiccant and, as a consequence, the numerical solution time are nearly doubled showing that the convergence limit in Eq. (62) is acceptable. The reader should be reminded that ΔC_{Salt} is considered zero in this study unless otherwise indicated. Therefore the energy and mass balance criteria [Eqs. (60) and (61)] will be used unless otherwise noted.

3. Verification and numerical results for a single heat exchanger

The numerical model developed as outlined above, is for the case of both heat and moisture transfer, however its accuracy is verified in this section with the case of only heat transfer in a single exchanger because this is the only available analytical solution. Romie [15] simplified the solution of transient response of cross-flow heat exchangers for the case of negligible thermal capacitance of the wall compared to the thermal capacitance of the fluids in the exchanger which is consistent with Assumption 5 in this paper. In Romie's study, the fluid capacitance rates, C_a and C_b, and the overall heat transfer coefficient (U) were assumed to be constant, which is consistent with the assumption used in the model developed in this thesis when there is no moisture transfer. In addition, there was no external heat transfer from the external surface of the exchanger ($\sigma = 0$ in this study). The fluids were unmixed and the analysis was based on ideal plug flow (Assumption 3 in this paper).

In this solution "x" is the distance from the fluid "a" entrance [corresponding to the air flow in Fig. 1(b)] entrance and the flow length is x_0; also, "y" is distance from the fluid "b" entrance [corresponding to the desiccant fluid flow in Fig. 1(b)] and the flow length is y_0. The dimensionless time ($t_a^* = tV_a/x_0$ and $t_b^* = tV_b/y_0$) for each stream are presented based on the times required for fluids "a" and "b" in the exchanger to be replaced by the input fluids flow similar to definition of dimensionless times for the (LAMEE) in this paper. For cross-flow exchangers, the time to reach a new steady-state condition due to a step change in one or two incoming fluid temperatures can be expressed by predefined dimensionless

times when the exchanger wall capacitance is negligible. Now the dimensionless variables $x^* = x/x_0$, $y^* = y/y_0$, $\tau^* = 1/(t_a^{*-1} + t_b^{*-1})$ and the dimensionless parameters $NTU_a = Ux_0y_0/C_a$, C_a/C_b and $\alpha = t_a^*/(t_a^* + t_b^*)$ can be defined. Romie [15] obtained the dimensionless fluid temperatures following a step perturbation of fluid "a" at time zero where dimensionless temperature is defined as:

$$\theta(\tau^*) = \frac{T - T_{b,in}}{T_{a,in} - T_{b,in}}, \tag{63}$$

In order to express the solution for differential equations, the Anzelius–Schuman functions, $G_0(\psi, \omega)$ and $F_0(\psi, \omega)$, and their extension were used. The transient response was obtained by the threefold Laplace transform. The temperature fields were obtained by inversion of the resulting Laplace equations. As the bulk mean outlet temperatures, $\theta_{a,out}(\tau^*)$ and $\theta_{b,out}(\tau^*)$, are of most interest heat exchanger analysis, Romie [15] presented these mean temperatures, which are calculated as follows:

$$\theta_{a,out}(\tau^*) = U(\tau^* - \alpha)\int_0^1 F_0\left(NTU_a, y'\frac{C_a}{C_b}NTU_a\right)dy^*, \tag{64}$$

where $y'=\min\left(y^*, \frac{(\tau^* - x^*\alpha)}{(1-\alpha)}\right)$, ($x^*=1$) and

$$\theta_{b,out}(\tau^*) = \int_0^{x'} G_0\left(x^*NTU_a, y'\frac{C_a}{C_b}NTU_a\right)dx^*, \tag{65}$$

where $x'=\min(1, \frac{\tau^*}{\alpha})$ and $y' = \min(y^*, \frac{(\tau^* - x^*\alpha)}{(1-\alpha)})$, ($y^*=1$).

This analytical solution can be used to validate the numerical model presented in this paper for the case of only heat transfer. Using a grid of 100×100 nodes, the numerical solution is very close to the analytical solution for the bulk outlet temperatures shown in Fig. 4. The comparison is made for $NTU_a = 2$, $C_a/C_b = 0.75$ and $\alpha = 1/2$.

From Fig. 4, it can be seen that numerical solution is in agreement with the analytical solution except for the temperature of fluid "a" over an interval near the time $\tau^* = \alpha = 0.5$. In the analytical solution, the fluid "a" exhibits a step response, when $\tau^* = \alpha$ and therefore $t = x_0/V_a$. This abrupt step change is due to the fact that the outlet temperature of fluid "a" cannot change until the fluid flow that enters at time zero with a step change in its temperature passes through the exchanger (i.e. at $t = x_0/V_a$). On the other hand, the outlet temperature of fluid "a" changes smoothly in the numerical model results. The reason for the observed behavior is a phenomenon called false diffusion. In this problem, it is expected that due to neglecting the axial dispersion in the direction of fluid flows, the outlet temperature of fluid "a" does not change until the perturbation in its inlet temperature is advected to the exit cross section of the channel. However, a backward scheme in the numerical solution causes an earlier change in the outlet temperature of fluid "a" due to numerical solution diffusion. It should be noted that the numerical results may be more physically realistic than the analytical results near this time because a small amount of diffusion would occur in reality.

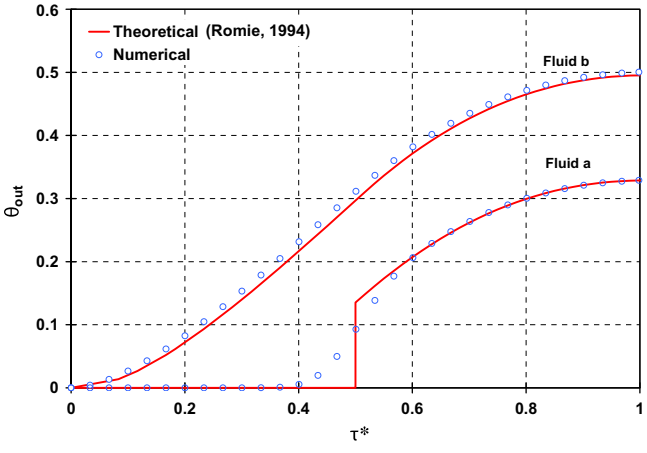

Fig. 4. Comparison between the bulk outlet temperature of a cross-flow heat exchanger calculated with the numerical model in this paper and the analytical solution [15] following a step change in fluid "a" at time zero ($NTU_a = 2$, $C_a/C_b = 0.75$ and $\alpha = 1/2$).

As shown in Fig. 4, the numerical diffusion causes a faster initial response at the outlet of fluid "a" temperature. This change in the initial response does not have influence on that the prediction of the transient response time of the exchanger ($\tau^* = 1$) and the quasi-steady state effectiveness values which are the main interest in this study. Moreover, this discrepancy occurs early in the transient period after a perturbation in fluid "a" temperature within a single heat exchanger which has a much lower transient response time compared to the RAMEE system containing a coupling fluid with a high thermal and mass transfer capacitance (see Part II). The numerical solution for fluid "a" agrees with the analytical solution within the error of ±1% outside the range of $0.4 < \tau^* < 0.6$, also the maximum discrepancy between the simulated bulk outlet temperature of fluid "b" and its theoretical value is 4% during the transient period. At quasi-steady state condition ($\tau^* = 1$), the discrepancy between numerical and analytical value of the dimensionless temperature of fluid "a" and fluid "b" is 0.007% and 1% respectively.

4. Experimental validation

In order to validate numerical model, the data from the numerical model are compared with data from a laboratory experiment on a RAMEE system comprising two LAMEEs and two storage tanks, one in each airstream.

4.1. RAMEE prototype

A RAMEE prototype was built and tested by Erb et al. [16]. The RAMEE consisted of two exchangers with 10 desiccant flow channels, separated from the airstream by a Propore™ membrane. The exchanger characteristics were identical to the characteristics given in Table 2. The exchangers were cross-flow in design, and a liquid $MgCl_2$ desiccant was pumped from the bottom of the exchanger to the top to ensure pressurization and better flow distribution. The test facility set up is similar to Fig. 1(a).

4.2. Transient experimental test setup

Testing the RAMEE system requires an experimental facility that provides two airstreams with well controlled temperature, humidity and flow rate. One airstream was designed to simulate outdoor air entering a building and was supplied from an environmental chamber. Constant airflow was provided by two vacuum pumps which were located both upstream and downstream of the supply exchanger, which provided equal pressures on either side. The exhaust airstream mass flow rate was identical to the supply airstream, except that the inlet air was taken from the laboratory room at standard room conditions. The airstream temperatures were measured on each side of both exchangers using both T-type thermocouples and resistance temperature detectors (RTD's). Humidity was also measured on each side of both exchangers using a capacitive humidity sensor. The mass flow rate of air was measured on both sides of each exchanger using an orifice plate and a differential pressure transducer. The orifice plates and piping were designed following ISO Standard 5167-1 [31]. $MgCl_2$ solution was supplied to each exchanger using a 0.092 kW (1/8th hp) magnetic drive pump, and the flow rate was measured

using a rotometer. To allow for fluctuations in desiccant volume due to changes in concentration, a storage tank was placed in the desiccant line after the outlet of each exchanger (see Fig. 2). These storage tanks and lines were insulated to reduce the heat gains/losses between the solution and the surroundings. The entire data acquisition was handled with the use of LabVIEW software, and data was collected at 10 second intervals.

4.3. Comparison of experimental results with theoretical predictions

The results from the numerical model are compared to the experimental measurements for both summer and winter operating conditions. This comparison requires the physical size and dimension of the exchangers, headers, storage tanks and piping as well as the heat loss/gain from/to the RAMEE system during the laboratory testing. The external heat gains/losses were estimated assuming steady state heat transfer from the RAMEE system based on the measured temperatures of the solution and the surroundings, and the size, material and insulation of the experiment (e.g., storage tanks, pipes and LAMEE headers). The value of σ depends on the test conditions and was estimated to be -0.1 and 0.45 for the supply side of the system and -0.1 and 0.85 for the system exhaust side during the summer and winter test conditions, respectively. This means the solution looses heat to the surroundings during the summer test conditions and gains heat from the surroundings during the winter test conditions. It

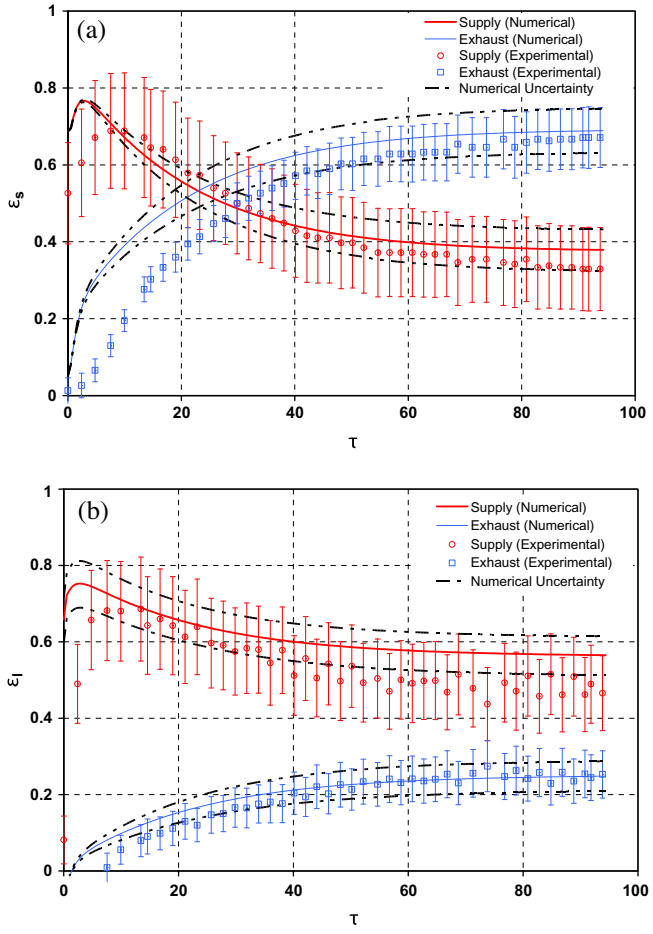

Fig. 5. Comparison of transient: (a) sensible and (b) latent effectivenesses calculated from numerical model with experimental data for RAMEE system (summer operating conditions, $NTU_S = NTU_E = 11.5$, $C_{Sol}/C_{Air} = 6.1$, $\mu = 0.15$, $\sigma_S = -0.1$, $\sigma_E = -0.1$, $\Delta C_{Salt} = 8\%$). (Error bars indicate the 95% uncertainty in measured data.)

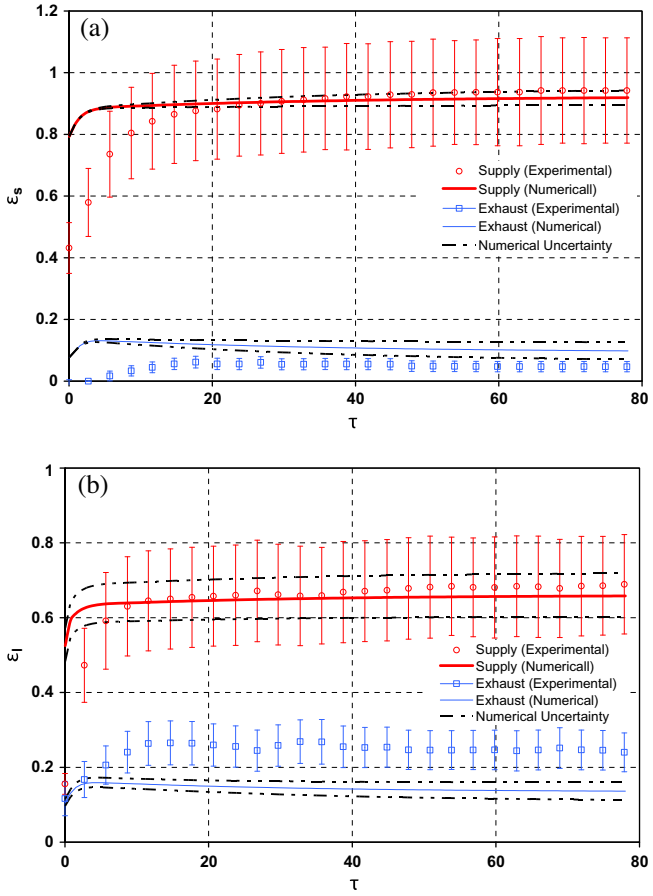

Fig. 6. Comparison of transient: (a) sensible and (b) latent effectivenesses calculated from numerical model with experimental data for RAMEE system (winter operating conditions, $NTU_S = NTU_E = 11.3$, $C_{Sol}/C_{Air} = 10.2$, $\mu = 0.15$, $\sigma_S = 0.45$, $\sigma_E = 0.85$, $\Delta C_{Salt} = -1\%$). (Error bars indicate the 95% uncertainty in measured data.)

needs to be mentioned that the test conditions (i.e., temperature and humidity ratio) are close to, but not exactly, AHRI test conditions due to restrictions in conditioning the air to precise values. However, the initial and boundary conditions are taken from the experimental measurements. The initial salt solution concentration ($C_{Salt,Initial}$) is reported to be (~34%) by weight in the laboratory testing. Knowing inlet air conditions in the supply and the exhaust side of the system, the steady date concentration of liquid desiccant can be calculated from the steady state model for the RAMEE system [13]. Therefore, the value of ΔC_{Salt} is obtained to be 8% and -1% during the summer and winter test conditions, respectively.

Figs. 5 and 6 show a numerical/experimental comparison of the transient effectiveness for heat and moisture transfer during summer and winter testing, respectively. The experimental data are presented along with their uncertainty limits in this comparison. The numerical uncertainties in Figs. 5 and 6 are determined considering the uncertainty of moisture diffusion resistance (δ/k_m) of the membrane and heat loss/gain ratio (σ). The reason for taking the uncertainty of moisture diffusive resistance into account for the comparison of the numerical model data and experimental measurements is the indication of sensitivity studies. Simulation results show that the moisture diffusion resistance of the membrane has the greatest influence (up to 0.06) on the predicted effectiveness of the RAMEE system relative to other simplifying assumptions and property data. The uncertainty of heat loss/gain ratio should be included in the comparison because the exact physical properties (e.g, wall thickness, thermal conductivity, diameter, length) of pipes, headers and reservoirs used to estimate

Table 3
The root mean square error (RMSE) and the average absolute difference of effectiveness values from the experimental comparison of the RAMEE system at summer and winter operating conditions.

		Supply sensible	Exhaust sensible	Supply latent	Exhaust latent
RMSE	Summer testing	0.044	0.097	0.088	0.035
	Winter testing	0.069	0.065	0.037	0.1
Average absolute difference	Summer testing	0.035	0.075	0.074	0.024
	Winter testing	0.037	0.062	0.025	0.103

the heat loss/gain from/to the liquid desiccant loop is unknown. The uncertainty of heat loss/gain ratio (φ_σ) is considered to be ±0.05.

The total uncertainty in predicted effectiveness will be a function of both the uncertainty of moisture diffusion resistance and the uncertainty of heat loss/gain ratio. Following ANSI/ASME PTS 19.1-1998, the uncertainty in the predicted transient effectiveness can be estimated as

$$\varphi_\varepsilon = \sqrt{(\varphi_{\delta/k_m})^2 + (\varphi_\sigma)^2} \tag{66}$$

As shown in Figs. 5 and 6 the effectiveness values from the numerical model are in good agreement with experimental data. The simulated effectivenesses show the same trend as the measured data. The sensible effectivenesses cross over in both simulated and experimental data at summer operating conditions as shown in Fig. 5. As illustrated in Fig. 6 for winter operating conditions, a divergence trend for supply side and exhaust side effectivenesses and higher difference between theses values compared to summer operating conditions were observed during laboratory testing of the RAMEE system. A similar trend is found from the simulation data for the same test condition.

In Figs. 5 and 6 for most of the transient times the agreement between simulated and experimental results is within the uncertainty limits. In addition, the model predicts very well the quasi-steady state effectiveness values and the simulated effectivenesses are well within the 95% uncertainty limits of the experiment data. The differences between the numerical and experimental data are mainly attributed to flow distribution problem within liquid channels in the experiment. In the exchangers designed by Erb et al. [16], the entrance of liquid channels does not have uniform thickness to distribute the liquid desiccant within the liquid channels evenly. As well, the thickness of liquid channels is not exactly the same in all the panels due to manufacturing variations. Additionally, the membrane deflections in the pressurized RAMEE system cause changes in the hydraulic diameter of the fluid channels. These problems in the design and construction of the exchangers are not addressed in this study.

As illustrated in Figs. 5 and 6, a discrepancy between the simulation and the experiment is observed at initial times. It is due to the fact that it will take time to fill the exchangers with the salt solution and also the exact initial conditions are difficult to determine.

During winter test conditions, heat gain from the environment has a significant influence on the transient behavior of the RAMEE system. As shown in Fig. 6, this phenomenon results in a large difference between the sensible effectivnesses of the supply and exhaust exchangers due to excessive addition of heat to the liquid desiccant from the surrounding. This results in high effectiveness values in the supply side while the exhaust side has much lower effectiveness values. As illustrated in Fig. 6, the aforementioned behavior also can be predicted by the numerical model and simulated values show good agreement with the measured values.

To have a better assessment of the comparison between the numerical and experimental data, the root mean square error (RMSE) for the prediction of simulation model is calculated as follows:

$$RMSE = \frac{\sqrt{\sum_1^N (\varepsilon_{\text{Simulation}} - \varepsilon_{\text{Experimental}})^2}}{N} \tag{67}$$

where N is the number of points in the transient solution used to compare the results. During summer and winter testing conditions, the value of RMSE for various effectiveness values are presented in Table 3. One may use these data to evaluate accuracy of a numerical model considering the influence of more parameters (e.g., non-uniform flow in the exchangers, possible crystallization of the salt solution on the membrane, etc.) on the RAMEE system performance when it is compared to the current model.

In addition to the RMSE, the average absolute difference is used to quantify the comparison between numerical and experimental data. This value is defined as

$$\text{Average Absolute Difference} = \frac{|\varepsilon_{\text{Simulation}} - \varepsilon_{\text{Experimental}}|}{N} \tag{68}$$

This average absolute difference for various effectiveness values is presented in Table 3. The maximum average absolute difference between the measured and simulated effectivenesses is 0.075 (i.e., exhaust sensible) and 0.103 (i.e., exhaust latent) for summer and winter operating conditions, respectively. These errors indicate that the prediction of numerical model is quite good and the validated model can be utilized to investigate the characteristics of the RAMEE system with various parameters and operating conditions.

5. Conclusion

In this work, a numerical model is developed to determine the transient behavior of a run-around membrane energy exchanger (RAMEE) system that consists of two cross-flow liquid-to-air membrane energy exchangers (LAMEEs) and two storage tanks; one in each side of the system. The effect of heat loss/gain from/to the liquid desiccant loop is considered in the numerical model, which can significantly impact the performance of the system. The detailed study of transient performance of the RAMEE is useful to determine the transient response time of the system and ways to control the RAMEE system under different practical situations.

The model for the case of only heat transfer for a single heat exchanger is compared to an available analytical solution and good agreement is obtained. It is shown that the discrepancy between the numerical model results and theoretical solution for the dimensionless bulk outlet temperature of fluids is less than 4% during the transient period. Also, a comparison between the numerical model and experimental measurements is presented for the case of simultaneous heat and moisture transfer during the laboratory testing of a RAMEE system. The results for both sensible and latent effectiveness showed satisfactory agreement at different operating conditions. However, there are some discrepancies between initial transient responses due to experimental flow distribution problems within exchanger. The maximum average absolute difference between the simulated and experimental data for the transient effectiveness is 0.103 which implies good accuracy of the numerical model for the RAMEE system with complex design characteristic and testing facilities. Further investigation should be conducted

to include mal-distribution in the numerical model to improve this agreement.

The numerical model developed and verified in this part of the paper can be used to investigate the various characteristics of the RAMEE system.

Acknowledgements

This research was financially supported by the National Science and Engineering Research Council of Canada (NSERC) and Venmar CES, Inc., Saskatoon, SK, Canada.

References

[1] ASHRAE, ASHRAE Handbook-Fundamentals 2005, American Society of Heating, Refrigerating and Air-Conditioning Engineers, Inc., Atlanta, 2005.
[2] M. Fauchoux, C.J. Simonson, D.A. Torvi, The effect of energy recovery on perceived air quality, energy consumption and economics of an office building, ASHRAE Trans. 113 (2) (2007) 437–449.
[3] J.M. Hill, S.M. Jeter, Use of heat pipe heat exchangers for enhanced dehumidification, ASHRAE Trans. 100 (1) (1994) 91–102.
[4] H. Fan, C.J. Simonson, R.W. Besant, Run-around heat recovery system using cross-flow flat-plate heat exchangers with aqueous ethylene glycol as the coupling fluid, ASHRAE Trans. 111 (1) (2005) 901–910.
[5] C.J. Simonson, D.L. Ciepliski, R.W. Besant, Determining the performance of energy wheels: Part I – experimental and numerical methods, ASHRAE Trans. 105 (1) (1999) 174–187.
[6] C.J. Simonson, D.L. Ciepliski, R.W. Besant, Determining the performance of energy wheels: Part II – experimental data and numerical validation, ASHRAE Trans. 105 (1) (1999) 188–205.
[7] G. Stiesch, S.A. Klein, J.W. Mitchell, Performance of rotary heat and mass exchangers, HVAC R Res. 1 (4) (1995) 308–323.
[8] M.S. Park, J.R. Howell, G.C. Vliet, Numerical and experimental results for coupled heat and mass transfer between a desiccant film and air in cross-flow, Int. J. Heat Mass Transfer 37 (1) (1994) 395–402.
[9] A. Ali, K. Vafai, A.-.A. Khaled, Analysis of heat and mass transfer between air and falling film in a cross flow configuration, Int. J Heat Mass Transfer 47 (4) (2004) 743–755.
[10] L.C.S. Mesquita, S.J. Harrison, D. Thomey, Modeling of heat and mass transfer in parallel plate liquid-desiccant dehumidifiers, Solar Energy 80 (11) (2006) 1475–1482.
[11] J.L. Niu, L.Z. Zhang, Membrane-based enthalpy exchanger: material considerations and clarification of moisture resistance, J. Membr Sci. 189 (2) (2001) 179–191.
[12] L.Z. Zhang, J.L. Niu, Effectiveness correlations for heat and moisture transfer processes in an enthalpy exchanger with membrane cores, J. Heat Transfer 124 (5) (2002) 922–929.
[13] H. Fan, C.J. Simonson, R.W. Besant, Performance of a run-around system for HVAC heat and moisture transfer applications using cross-flow plate exchangers coupled with aqueous lithium bromide, HVAC R Res. 12 (2) (2006) 313–336.
[14] M.D. Larson, C.J. Simonson, R.W. Besant, The elastic and moisture transfer properties of polyethylene and polypropylene membranes for use in liquid-to-air energy exchangers, J. Membr Sci. 302 (1) (2007) 136–149.
[15] F.E. Romie, Transient response of crossflow heat exchangers with zero core thermal capacitance, J. Heat Transfer 116 (3) (1994) 775–777.
[16] B. Erb, M. Seyed Ahmadi, C.J. Simonson, R.W. Besant, Experimental measurements of a run-around membrane energy exchanger (RAMEE) with comparison to a numerical model, ASHRAE Trans. (2009).
[17] C.R. Iskra, C.J. Simonson, Convective mass transfer coefficient for a hydrodynamically developed airflow in a short rectangular duct, Int. J. Heat Mass Transfer 50 (11) (2007) 2376–2393.
[18] X. Luo, W. Roetzel, Theoretical investigation on cross-flow heat exchangers with axial dispersion in one fluid, Revue Générale De Thermique 37 (3) (1998) 223–233.
[19] M. Mishra, P.K. Das, S. Sarangi, Transient behavior of crossflow heat exchangers with longitudinal conduction and axial dispersion, J. Heat Transfer 126 (3) (2004) 425–433.
[20] C.J. Simonson, R.W. Besant, Heat and moisture transfer in desiccant coated rotary energy exchangers: Part I: numerical model, HVAC R Res. 3 (4) (1997) 325–350.
[21] C. Iskra, Convective mass transfer between a hydrodynamically developed airflow and liquid water with and without a vapor permeable membrane, M.Sc. thesis, University of Saskatchewan, Saskatoon, Saskatchewan, 2007.
[22] L.A. Cisternas, E.J. Lam, Analytic correlation for the vapour pressure of aqueous and non-aqueous solutions of single and mixed electrolytes. Part II: application and extension, Fluid Phase Equilib. 62 (1) (1991) 11–27.
[23] I.D. Zaytsev, G.G. Aseyev, Properties of Aqueous Solutions of Electrolytes, CRC Press, Inc., Boca Raton, 1992.
[24] R.K. Shah, S. Kakaç, A.E. Bergles, F. Mayinger, Thermal design theory for regenerators, in: Heat Exchangers: Thermal-Hydraulic Fundamentals and Design. Hemisphere, New York, 1981 pp. 721–763.
[25] ANSI/AHRI Standard 1060-2005, Standard for Rating Air-to-Air Exchangers for Energy Recovery Ventilation Equipment, Air-Conditioning and Refrigeration Institute, Arlington.
[26] G. Stephanopoulos, Chemical Process Control: An Introduction to Theory and Practice, Englewood Cliffs, NJ, Prentice-Hall, 1984.
[27] F.P. Incropera, D.P. Dewitt, Fundamentals of Heat and Mass Transfer, John Wiley & Sons, New York, 2002.
[28] J.R. Welty, C.E. Wicks, R.E. Wilson, Fundamentals of Momentum, Heat and Mass Transfer, John Wiley & Sons Inc., New York, 2001.
[29] M. Gryta, Influence of polypropylene membrane surface porosity on the performance of membrane distillation process, J. Membr Sci. 287 (1) (2007) 67–78.
[30] N.T. Charles, D.W. Johnson, The occurrence and characterization of fouling during membrane evaporative cooling, J. Membr Sci. 319 (1) (2008) 44–53.
[31] ISO, Measurement of fluid flow by means of pressure differential devices, ISO 5167-1, Switzerland 1991.
[32] M. Seyed-Ahmadi, B. Erb, C.J. Simonson, R.W. Besant, Transient behavior of run-around heat and moisture exchanger system. Part II: Sensitivity studies for a range of initial conditions, Int. J. Heat Mass Transfer (2009), doi:10.1016/j.ijheatmasstransfer.2009.06.037.